

# PHASE-MIXING IN DISSIPATIVE ALFVÉN WAVES

JACK IRELAND and ERIC R. PRIEST

*School of Mathematical and Computational Sciences, University of St. Andrews,  
St. Andrews KY16 9SS, U.K.*

(Received: 7 August 1996; accepted: 22 November 1996)

**Abstract.** The phase-mixing mechanism first proposed as a coronal heating mechanism by Heyvaerts and Priest (1983) is examined using a length-scale analysis adapted from Cally (1991). This allows parameter ranges other than those studied by Heyvaerts and Priest (1983) to be described, together with a detailed examination of the transfer of energy to both longer and shorter length-scales as the Alfvén wave front evolves in the solar corona. The results of Heyvaerts and Priest (1983) are largely confirmed, but with some notable differences. Energy initially at smaller length-scales decays faster than their rate, because the plasma is more strongly dissipative at smaller length-scales. The full inclusion of diffusion across field lines also leads to smoother Alfvén wavefronts.

## 1. Introduction

Phase-mixing was first proposed as a possible coronal heating mechanism by Heyvaerts and Priest (1983) where the evolution of Alfvén waves in a magnetically open region was considered (as well as in a closed region). The background Alfvén speed  $v_A^2(x)$  was assumed to be a function of  $x$  alone and has gradients in the  $\hat{x}$ -direction (Figure 1). The inhomogeneity in the background Alfvén speed means that Alfvén waves on neighbouring field lines have different wavelengths. Therefore, as the wave progresses in  $z$ , waves on neighbouring field lines move out of phase relative to each other. The effect of this inhomogeneity is easily demonstrated in the wave equation

$$\frac{\partial^2 v}{\partial t^2} = v_A^2(x) \frac{\partial^2 v}{\partial z^2}, \quad (1)$$

which describes phase-mixing in a non-dissipative system. A solution is

$$v \sim \exp[-i(\omega t + k(x)z)], \quad (2)$$

for a wave of frequency  $\omega$ , where  $k(x) = \omega/v_A(x)$ , so that

$$\frac{\partial v}{\partial x} \sim v z \frac{dk}{dx}. \quad (3)$$

The inclusion of a non-uniform background Alfvén velocity therefore creates gradients in the  $x$ -direction that increase with  $z$ . Note also that sharper gradients appear at lower heights for a more inhomogeneous plasma through the gradient of  $k(x)$ .

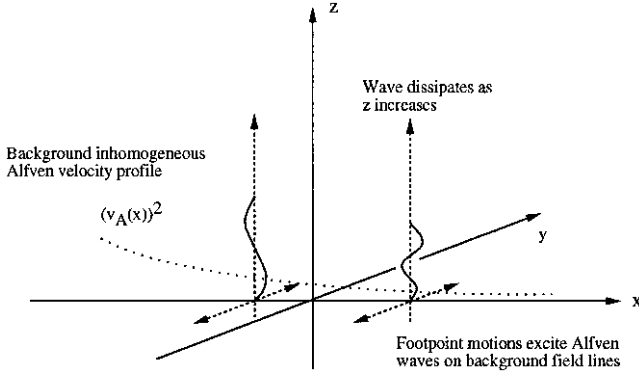


Figure 1. Heyvaerts and Priest (1983) model of phase-mixing.

It is these large gradients that will be substantially affected by the presence of dissipation in the plasma.

Following Heyvaerts and Priest (1983), we adopt a simple model of phase-mixing in which a vertical magnetic field has its photospheric footpoints oscillated at frequency  $\omega$ . The equilibrium is taken as

$$\mathbf{B}_0 = B_0(x)\hat{\mathbf{z}}, \quad \rho_0 = \rho_0(x), \quad (4)$$

where  $\mathbf{B}_0$  is the background magnetic field and  $\rho_0$  the fluid density profile. We consider perturbations  $v(x, z, t)$  and  $b(x, z, t)$  in the velocity and magnetic fields, respectively, only in the  $y$ -direction so that phase-mixing of Alfvén waves is produced. After linearisation of the equations of motion and the induction equation respectively, we obtain

$$\rho_0 \frac{\partial v}{\partial t} = \frac{B_0}{\mu} \frac{\partial b}{\partial z} + \rho_0 \nu_v \nabla^2 v \quad (5)$$

and

$$\frac{\partial b}{\partial t} = B_0 \frac{\partial v}{\partial z} + \nu_m \nabla^2 b, \quad (6)$$

where  $\nu_m$  is the magnetic diffusivity and  $\nu_v$  is the kinematic viscosity. These can be combined to give

$$\frac{\partial^2 v}{\partial t^2} = v_A^2(x) \frac{\partial^2 v}{\partial z^2} + (\nu_m + \nu_v) \left( \frac{\partial^2}{\partial x^2} + \frac{\partial^2}{\partial z^2} \right) \frac{\partial v}{\partial t}, \quad (7)$$

where  $v_A^2(x) = B_0^2/[\mu\rho_0(x)]$  is the Alfvén speed squared. The two important terms for phase-mixing in Equation (7) are the wave term  $v_A^2(x) \partial^2 v/\partial z^2$  and the damping term  $\partial^3 v/\partial t \partial x^2$ . The first term indicates that the wavelength is different on each field line and this generates the large horizontal gradients that are damped by the second term. The  $\partial^3 v/\partial t \partial z^2$  term in (7) is not important for phase-mixing and will be neglected from now on so that we adopt as our basic equation

$$\frac{\partial^2 v}{\partial t^2} = v_A^2(x) \frac{\partial^2 v}{\partial z^2} + (\nu_m + \nu_v) \left( \frac{\partial^2}{\partial x^2} \right) \frac{\partial v}{\partial t}. \quad (8)$$

In their analysis, Heyvaerts and Priest (1983) assume a solution to Equation (8) of the form

$$v \sim \hat{v}(x, z) \exp[-i(\omega t + k(x)z)]. \quad (9)$$

They also assume *weak damping*,

$$\frac{1}{k} \frac{\partial}{\partial z} \ll 1, \quad (10)$$

and *strong phase-mixing*,

$$\frac{z}{k} \frac{\partial k}{\partial x} \gg 1, \quad (11)$$

conditions that are most likely to exist in the solar corona. Under these assumptions, they establish the solution

$$\hat{v}(x, z) = \hat{v}(x, 0) \exp \left[ -\frac{1}{6} \left( \frac{k(x)z}{R_{\text{Tot}}^{1/3}} \right)^3 \right], \quad (12)$$

where

$$R_{\text{Tot}} = \frac{\omega}{\nu_m + \nu_v} \left( \frac{d}{dx} \log k(x) \right)^2. \quad (13)$$

Their analysis indicates that Alfvén waves will decay as  $\exp(-z^3)$  under likely coronal conditions. Note, however, that this solution is only valid under the conditions described above: in particular, it is not appropriate at small  $z$  where condition (11) fails.

Refinements to this analysis do already exist; in particular, Browning and Priest (1984) looked at the effect of the Kelvin–Helmholtz instability on phase-mixing and found that this may enhance the decay rate. Nocera, Leroy, and Priest (1984) examined phase-mixing in propagating Alfvén waves and found evidence for an  $\exp(-z^3)$  behaviour at large heights. Also, Hood, Ireland, and Priest (1997) have shown that Equation (8) has a similarity solution for a background Alfvén velocity  $v_A^2 \sim \exp(x/a)$  and that this solution does indeed exhibit the characteristic  $\exp(-z^3)$  for the Heyvaerts–Priest conditions, (10) and (11). It seems therefore that this decay  $\exp(-z^3)$  is a very robust feature in solutions to Equation (8) for very different analyses when conditions (10) and (11) are imposed. Our aim in this paper is to investigate the process of phase-mixing in more detail by extending the

Heyvaerts and Priest (1983) analysis to other possible conditions (such as, weak phase-mixing and weak damping).

## 2. Solution Technique

Following Cally (1991), Equation (8) is solved by assuming a harmonic time dependence, i.e.,  $v(x, z, t) = \exp(-i\omega t)u(x, z)$  and a solution in the space variables on  $0 < x < L$ ,  $0 \leq z < \infty$  of the form

$$u(x, z) = \sum_{n=1}^{\infty} A_n(z) \sin\left(\frac{n\pi x}{L}\right) \quad (14)$$

with

$$v_{\text{A}}^2(x) = v_0^2 \left[ 1 + \sum_{n=1}^{\infty} P_n \cos\left(\frac{n\pi x}{L}\right) \right], \quad (15)$$

where  $v_0^2$  is the uniform background Alfvén velocity. We take our boundary conditions as  $v(0, z, t) = v(L, z, t) = 0$  with  $u(x, 0) = F(x) = \sum_{n=1}^{\infty} F_n \sin(n\pi x/L)$  and  $u(x, z) \rightarrow 0$  as  $z \rightarrow \infty$ .

This leads to an infinite set of coupled ordinary differential equations of the form

$$A_n K_n^2 + \frac{1}{k_0^2} A_n'' + \frac{1}{2k_0^2} \sum_{m=1}^{\infty} P_m [A_{n+m}'' + A_{n-m}'] = 0, \quad (16)$$

where  $K_n^2 = 1 + i[n\pi\Lambda/L]^2$ ,  $\Lambda^2 = (\nu_m + \nu_v)/\omega$ , and  $1/k_0^2 = v_0^2/\omega^2$ .  $\Lambda$  is the dissipative length-scale for the system, which allows us to define a Reynolds number ( $R = L^2/\Lambda^2$ ) that we use to characterise dissipation in the system.

We next assume that  $A_n = a_n \exp(pz)$ , which leads to an infinite set of coupled difference equations, namely,

$$a_n K_n^2 + \frac{p^2}{k_0^2} a_n + \frac{p^2}{2k_0^2} \sum_{m=1}^{\infty} P_m [a_{n+m} + a_{n-m}] = 0. \quad (17)$$

These can be written in matrix form as

$$\left[ \mathbf{N} + \frac{1}{2} \mathbf{P} \right] \mathbf{a} = \left\{ -\frac{1}{q^2} \right\} \mathbf{K}^2 \mathbf{a}, \quad (18)$$

where  $q^2 = p^2/k_0^2$ ,  $\mathbf{N} = \mathbf{I}\{[k_0^2/\omega^2 L] \int_0^L v_{\text{A}}^2(x) dx\}$ ,  $\mathbf{a}^T = (a_1, a_2, a_3, \dots)$ ,  $\mathbf{K}^2 = \text{diag}(K_1^2, K_2^2, K_3^2, \dots)$ , and

$$\mathbf{P} = \begin{bmatrix} 0 & P_1 & P_2 & P_3 & \cdots \\ P_1 & 0 & P_1 & P_2 & \cdots \\ P_2 & P_1 & 0 & P_1 & \cdots \\ P_3 & P_2 & P_1 & 0 & \cdots \\ \vdots & \vdots & \vdots & \vdots & \ddots \end{bmatrix} \quad (19)$$

is the phase-mixing matrix. Elements above the leading diagonal couple long length-scales to shorter ones, while elements below the leading diagonal perform the reverse process. This means energy that has been phase-mixed down to short length-scales can wash back up the Alfvén wavefront to produce longer length-scales.

Rewriting (18) we find

$$\left\{ \mathbf{K}^{-1} \left[ \mathbf{N} + \frac{1}{2} \mathbf{P} \right] \mathbf{K}^{-1} \right\} \{ \mathbf{K} \mathbf{a} \} = \left\{ -\frac{1}{q^2} \right\} \{ \mathbf{K} \mathbf{a} \}, \quad (20)$$

which is an eigenproblem of the form

$$\mathbf{M} \mathbf{e} = \lambda \mathbf{e}, \quad (21)$$

where  $\lambda = -1/q^2$ ,  $\mathbf{M} = \mathbf{K}^{-1} [\mathbf{N} + \frac{1}{2} \mathbf{P}] \mathbf{K}^{-1}$  and  $\mathbf{e} = \mathbf{K} \mathbf{a}$ .  $\mathbf{M}$  and  $\mathbf{e}$  are both infinite but are truncated to some finite size to render them computationally tractable (see Section 4).

Having solved the eigenproblem, and assuming the eigenvalues to be distinct, the solution may then be reconstructed to give the general solution of (16) as

$$A_m(z) = K_m^{-1} \sum_{n=1}^{\infty} S_{mn} [c_n \exp(p_n z) + d_n \exp(-p_n z)], \quad (22)$$

where  $S_{mn}$  is the  $m$ th component of the  $n$ th eigenvector of  $\mathbf{M}$ . Initial conditions are found by solving the equations

$$\mathbf{S}[\mathbf{c} + \mathbf{d}] = \mathbf{K} \mathbf{f}(0), \quad (23)$$

where  $\mathbf{S}$  is the matrix  $[S_{mn}]$ ,  $\mathbf{c} = [c_1, c_2, c_3, \dots]^T$ ,  $\mathbf{d} = [d_1, d_2, d_3, \dots]^T$ , and condition  $\mathbf{f}(0) = (F_1, F_2, F_3, \dots)$ . Each component of the solution of this set of linear equations has the form  $c_n + d_n = f_n$  for some  $f_n$ . The boundary condition at infinity allows one to assign either  $c_n$  or  $d_n$  to  $f_n$ . If the real part of  $p_n$  is positive then the boundary condition at infinity implies that  $c_n = 0$ , so that we can put  $d_n = f_n$ . Similarly, if the real part of  $p_n$  is negative,  $d_n = 0$  and  $c_n = f_n$ . The kinetic energy in each Fourier mode is proportional to  $a_m(z) a_m^*(z)$ .

If we define

$$\phi_n(x) = \sum_{m=1}^{\infty} K_m^{-1} S_{mn} \sin\left(\frac{m\pi x}{L}\right), \quad (24)$$

then the overall solution may finally be written as

$$u(x, z) = \sum_{n=1}^{\infty} [c_n \exp(p_n z) + d_n \exp(-p_n z)] \phi_n(x), \quad (25)$$

from which it can be seen that the modes  $\phi_n(x)$  oscillate independently of each other.

### 3. Reduced Cases

It is instructive to consider first some reduced cases in order to gain insight into the two processes we are examining, namely phase mixing and dissipation.

#### 3.1. ZERO DISSIPATION

When  $\nu_m, \nu_v$  are identically zero we simply have the wave equation (1) to solve. For illustrative purposes, we consider a background Alfvén velocity of the form  $v_A^2(x) = v_0^2[1 + \delta \cos(x)]$ , where  $0 \leq \delta < 1$ . On substitution into (1) we obtain an infinite set of coupled ordinary differential equations of the form

$$A_n + \frac{1}{k_0^2} A_n'' + \frac{\delta}{2k_0^2} [A_{n+1}'' + A_{n-1}''] = 0. \quad (26)$$

We then assume that  $A_n = a_n \exp(pz)$ , which leads to an infinite set of coupled difference equations, namely

$$a_n + q^2 a_n + \delta \frac{q^2}{2} [a_{n+1} + a_{n-1}] = 0. \quad (27)$$

The eigenproblem becomes

$$\mathbf{M}_0 \mathbf{a} = - \left[ \frac{1}{q^2} \right] \mathbf{a} = \xi \mathbf{a}, \quad (28)$$

where  $\mathbf{a}^T = (a_1, a_2, a_3, \dots)$  and

$$\mathbf{M}_0 = \begin{bmatrix} 1 & \delta/2 & 0 & 0 & \cdots \\ \delta/2 & 1 & \delta/2 & 0 & \cdots \\ 0 & \delta/2 & 1 & \delta/2 & \cdots \\ 0 & 0 & \delta/2 & 1 & \cdots \\ \vdots & \vdots & \vdots & \vdots & \ddots \end{bmatrix}. \quad (29)$$

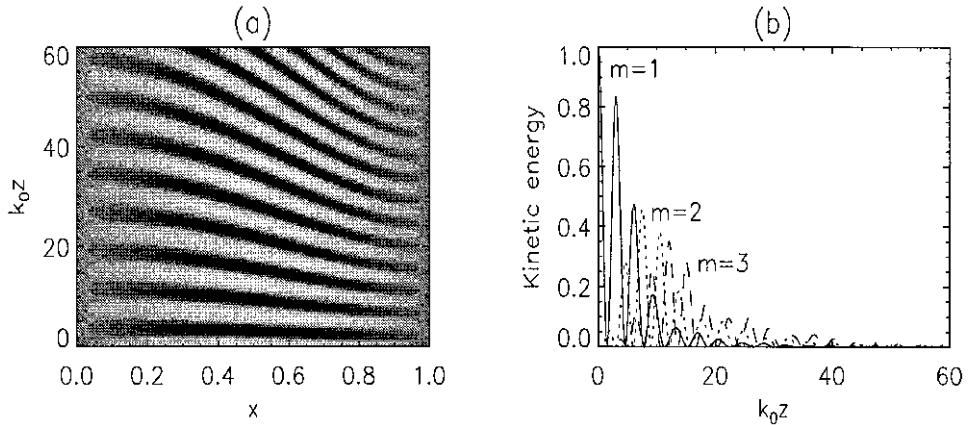


Figure 2. (a) Alfvén wave contour plot. Lighter tones represent wave peaks, darker tones wave troughs. (b) Length-scale excitation of first three length-scales in (a), as a function of  $k_0z$ .

When  $\mathbf{M}_0$  is finite (say, an  $N \times N$  matrix), this eigenvalue problem has an analytical solution, with the  $n$ th eigenvalue given by

$$\xi_n = -\frac{1}{q_n^2} = 1 + \delta \cos\left(\frac{n\pi}{N+1}\right) \quad (30)$$

for  $1 \leq n \leq N$ . The corresponding eigenvector is

$$\mathbf{a}_n = \left[ \sin\left(\frac{n\pi}{N+1}\right), \sin\left(\frac{2n\pi}{N+1}\right), \sin\left(\frac{3n\pi}{N+1}\right), \dots, \sin\left(\frac{Nn\pi}{N+1}\right) \right]. \quad (31)$$

(The matrix  $[\mathbf{S}_0]_{mn} = \sin\{nm\pi/(N+1)\}/\sqrt{N+1}$  whose columns consist of the orthonormal eigenvectors of  $\mathbf{M}_0$  will be used later.)

The effect of phase-mixing can be seen in Figures 2(a) and 2(b), where we have assumed  $u(x, 0) = \sin(x)$  and  $\delta = 0.5$ . As the wave progresses in the  $z$ -direction, the wavefront (and indeed, any line of constant phase) turns due to each field line in the plasma having a slightly different wavelength. At any cross section in the wavefront one can see that shorter length-scales are being created by phase mixing, due to the wavefront turning and so creating smaller length-scales in any  $x$ -directed cross-section. Figure 2(b) describes the appearance of Fourier modes  $m = 1, 2, 3, 4$  and  $5$  in the plasma from an energy point of view. At  $z = 0$ , all the energy is in the longest length-scale, Fourier mode  $m = 1$ . As  $z$  increases, other modes are excited. At  $k_0z \sim 1.4$ , the energy in  $m = 1$  is zero, but it then increases to a non-zero value due to energy being passed back to longer length-scales. At all length-scales energy is being transferred up to longer length-scales and down to shorter length-scales; mathematically, this is due to the sub- and super-diagonal terms in  $\mathbf{M}_0$  coupling energy from one length-scale to its two nearest neighbours.

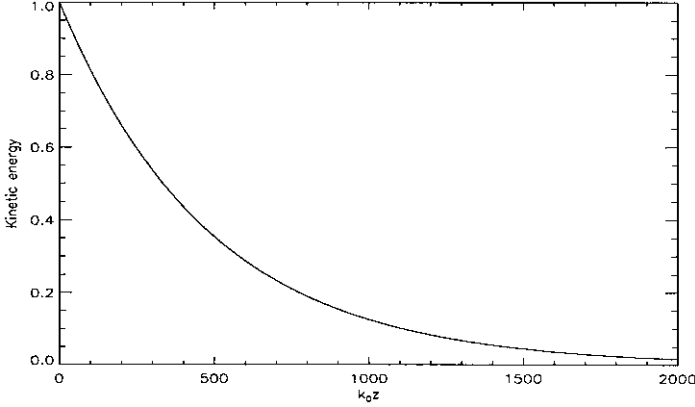


Figure 3. Energy dissipation of Fourier mode  $m = 1$  (solid line) in a uniform plasma.

As  $z$  increases, shorter and shorter length-scales are continually being excited. As the total amount of energy is constant this means that longer length-scales must be losing energy to the shorter ones. Even though all length-scales are being excited and de-excited the preferred direction of this energy transfer is towards shorter length-scales. Qualitatively, one can see from the  $\partial^3 v / \partial^2 x \partial t$  term in Equation (8) that these shorter length-scales will dissipate quicker than longer length-scales, enhancing the overall dissipation rate.

### 3.2. UNIFORM BACKGROUND FIELD

In this particular case we set  $v_A^2(x) = v_0^2$ , for which a very simple matrix equation is obtained, namely

$$\mathbf{M}_1 \mathbf{a} = - \left[ \frac{1}{q^2} \right] \mathbf{a} = \zeta \mathbf{a}, \quad (32)$$

where  $\mathbf{M}_1 = \text{diag}(K_1^2, K_2^2, K_3^2, \dots)$ . The phase-mixing matrix  $\mathbf{P}$  is identically zero and hence there is no coupling. Every length-scale therefore acts independently of every other one. For a finite matrix  $\mathbf{M}_1$  of size  $N \times N$

$$\zeta_n = -\frac{1}{q_n^2} = 1 + i \left( \frac{n\pi\Lambda}{L} \right)^2, \quad (33)$$

$1 \leq n \leq N$ . The eigenvectors are equally simple and form an array  $\mathbf{S}_1$  such that  $[\mathbf{S}_1]_{mn} = \delta_{mn}$ , where  $\delta_{mn}$  is the Kronecker delta. This reduced case implies that every length-scale is damped to some extent, not just the dissipative scales. Therefore as  $z$  increases, energy leaks out of each length-scale into the plasma.

Figure 3 shows the energy evolution experienced by an initial Alfvén wave profile  $v(x, 0) = \sin(\pi x)$  at  $R = 5000$  on  $0 \leq x \leq 1$  and  $0 \leq k_0 z \leq 2000$  in an

uniform plasma. As there is no phase-mixing, all the energy will stay in the initial Fourier mode and the decay is purely exponential with height; as can be seen, one needs to go to very large heights (in comparison to a non-uniform plasma – see Section 4) to obtain significant dissipation. If we include qualitatively the effects of phase-mixing, we see that the energy in the wave must dissipate faster whenever the plasma is non-uniform. Phase-mixing creates small length-scales, which according to Equation (33), have larger dissipation rates. This allows energy to dissipate from the wave faster than if all the energy had stayed at the same Fourier length-scale. Hence we have two competing processes: phase-mixing, which creates small length-scales, and dissipation, which acts to remove small length-scales from the plasma. The next section describes the effect of combining these processes on the energy dissipation rate in the Alfvén wave.

#### 4. General Results

The evolution of Alfvén waves of frequency  $\omega = 1$  is calculated on a background Alfvén velocity profile of the form

$$v_A^2(x) = v_0^2 \left[ 1 + \delta \cos \left( \frac{m\pi x}{L} \right) \right] \quad (34)$$

in the range  $0 \leq x \leq 1$  (i.e.,  $L = 1$ ). The ratio between maximum and minimum Alfvén velocities is  $\sqrt{(1+\delta)/(1-\delta)}$ . Heyvaerts and Priest (1983) describe points in the Alfvén wavefront where

$$\frac{z}{L_{ph}(x)} \gg 1 \quad (35)$$

as being strongly phase-mixed, where

$$L_{ph}(x) = \left[ \frac{1}{k(x)} \frac{dk(x)}{dx} \right]^{-1} = \frac{L}{2\pi\delta m} \left[ \frac{1 + \delta \cos \left( \frac{m\pi x}{L} \right)}{\sin \left( \frac{m\pi x}{L} \right)} \right] \quad (36)$$

for the profile equation (34); note also that  $\min[L_{ph}(x)] = (L/2\pi\delta m)\sqrt{1-\delta^2}$  at  $x = (L/m\pi) \cos^{-1}(-\delta)$ .  $L_{ph}(x)$  is a measure of the rate of creation of length-scales by the phase-mixing profile. The condition (35) implies that phase-mixing is well developed in the Heyvaerts and Priest solution –  $z$  is large compared to  $L_{ph}(x)$  and so short length-scales are well developed in the plasma. It also suggests that some points in the wavefront will be more highly phase-mixed than others.

The results of Section 3.2 confirm naturally that shorter length-scales in the plasma are dissipated more strongly than those at longer length-scales. Hence the degree to which an Alfvén wavefront is damped depends on what length-scales are present in the system. Heyvaerts and Priest (1983) assumed that

$$\frac{1}{k(x)} \frac{\partial}{\partial z} \ll 1 \quad (37)$$

in generating their solution (12), which implies that the presence of dissipation does not change the wavelength in the wavefront by very much.

In the following we shall take Equation (35) as the definition of strong phase-mixing, while weak phase-mixing corresponds to this condition not being fulfilled. Similarly, weak damping is described by Equation (37).

The damping strength can also be measured by considering the Reynolds number, which is a vital parameter since it controls the size of the matrix needed in order to resolve the Alfvén wave adequately. Since we intend to model dissipative processes, it would appear at first sight that resolution of the dissipative length-scale is necessary. One can estimate the value of  $N$  at which one would expect dissipative effects to be significant by considering the value of  $K_N^2$ : its complex part represents the dissipation present in the system and is of order unity when

$$N_{\min} \sim \frac{\sqrt{R}}{\pi}. \quad (38)$$

We assume that  $N \gtrsim N_{\min}$  is enough to resolve adequately the system. If we choose  $N$  too low, then a significant amount of energy will propagate down to the shortest available length-scale and bounce back up before dissipation becomes significant. This is obviously unphysical and can be checked *a posteriori*. For example for  $R = 5 \times 10^3$ , we require  $N \gtrsim 23$ . For such small values of  $N$  one can use standard numerical routines.

For illustrative purposes, we may assume that  $R = 5000$  represents a weakly damped plasma, and  $R = 50$  a strongly damped plasma. Approximate answers for larger values of  $R$  are achievable by the techniques described below – see Section 4.4.

#### 4.1. WEAK PHASE-MIXING

Weak phase-mixing arises when the plasma is almost uniform, for which we expect the Alfvén wave should not develop short length-scales very quickly. In this section we use Equation (34) as our phase-mixing profile with  $\delta = 0.0035$  and  $m = 1$ ; i.e., nearest neighbouring length-scale coupling. The Alfvén wave initial profile is  $u(x, 0) = \sin(\pi x)$  so that all the energy starts off in the longest length-scale.

##### 4.1.1. Weak Damping

It is sufficient for our purposes to take  $R = 5000$  as representing weak damping. The energy evolution for this wave (solid line) is shown in Figure 4(a), calculated with  $N = 52$ . The short-dashed line represents the zero-damping, constant energy case. The dash-dot-dot-dot line is the energy decay as calculated from the Heyvaerts–Priest solution. Also included for comparison is the energy decay for the same

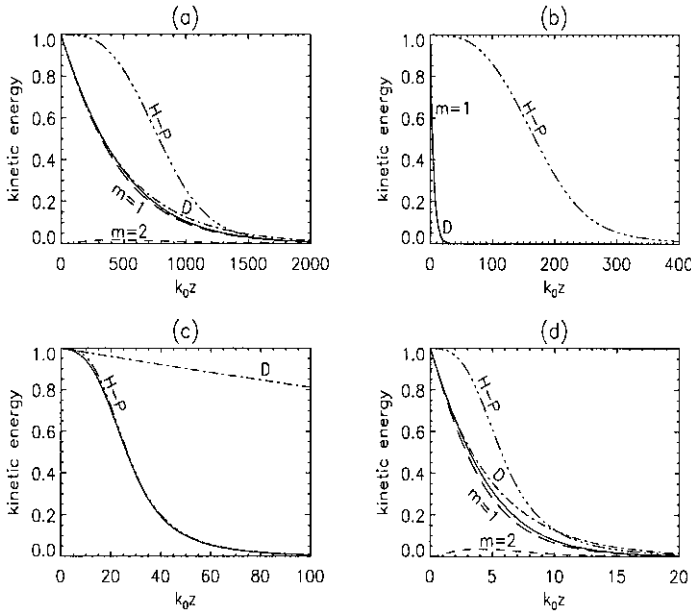


*Figure 4.* Results for (a) weak phase-mixing, weak damping, (b) weak phase-mixing, strong damping, (c) strong phase-mixing, weak damping, and (d) strong phase-mixing and strong damping. Key to plotted lines: Heyvaerts–Priest decay (H–P, dot-dot-dot-dashed line), uniform dissipative plasma (D, dot-dashed line), newly calculated answer (solid line), first Fourier mode  $m = 1$  (long-dashed line), and the second Fourier mode  $m = 2$  (short-dashed line)

wave profile in a uniform plasma (dot-dashed line). As can be seen, the wave decays almost as if the plasma were uniform, implying that phase-mixing is weak. Most of the energy is contained in the first Fourier mode (long-dashed line) but some is present in the second (short-dashed line) Fourier mode. Therefore energy is not being transferred in significant amounts down to shorter length-scales – the plasma is basically uniform.

The disparity at low  $z$  between the Heyvaerts–Priest solution and the one presented here can be explained by examining Equation (11). Since phase-mixing is weak, the phase-mixing length  $L_{ph}(x)$  is very long and hence large  $z$  is required to satisfy the strong phase-mixing condition, i.e., we need a large value of  $z$  to generate enough fine length-scales in the plasma for the overall decay to exhibit  $\exp(-z^3)$  behaviour.

However, this calculation shows that over the same range in  $z$ , the damping in the first Fourier mode is large enough to cause significant decay without recourse to phase-mixing. Hence in weakly inhomogeneous plasmas, as expected, the Heyvaerts–Priest  $\exp(-z^3)$  decay is not found.

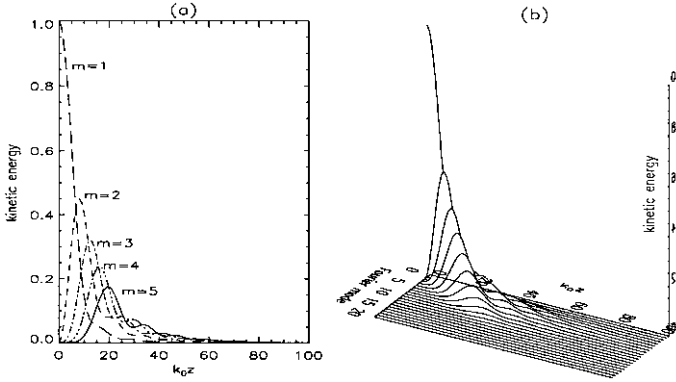


Figure 5. (a) Length-scale excitation in a strongly phase-mixed, weakly damped Alfvén wave. Fourier modes  $m = 1$  (long dashed line),  $m = 2$  (short dashed line),  $m = 3$  (dot-dashed line),  $m = 4$  (dot-dot-dot-dashed line), and  $m = 5$  (solid line) are shown. (b) Energy-mode-height diagram for a strongly phase-mixed, weakly damped Alfvén wave.

#### 4.1.2. Strong Damping

These conditions represent the opposite of the Heyvaerts–Priest analysis. Figure 4(b) shows the energy evolution for the Alfvén wave when  $R = 50$ . Such strong damping increases the dissipation of the wave, the net result being that the wave is damped very quickly (solid line). There are actually two other curves plotted very close to the true energy decay, these being the energy in the first Fourier mode and the uniform decay rate predicted by Equation (33), but they are indistinguishable from each other. In such a plasma we can say that the wave evolution is dissipative and phase mixing is unimportant. The damping in this system is too strong to allow phase-mixing to create smaller length-scales fast enough to affect the overall decay rate significantly.

### 4.2. STRONG PHASE-MIXING

In the following we consider Equation (34) with  $\delta = 0.5$ ,  $m = 1$  and initial conditions  $u(x, 0) = \sin(\pi x)$ . This value of  $\delta$  implies that the background Alfvén velocity changes by a factor of  $\sqrt{3}$  from  $x = 0$  to  $x = 1$ .

#### 4.2.1. Weak Damping

These are the conditions studied by Heyvaerts and Priest (1983). The calculated energy evolution of the Alfvén wave (solid line) is compared to the Heyvaerts–Priest (dot-dot-dot-dashed line) and uniform (dot-dashed line) energy evolution in Figure 4(c). The Heyvaerts–Priest solution is in good agreement with the calculated energy evolution, and both decay very much faster than the uniform case. Close to  $z = 0$  the energy evolution is basically dissipative. This is because phase-mixing has not yet created short enough length-scales with sufficient energy to affect the energy behaviour significantly: phase-mixing needs heights large compared to

$L_{ph}(x)$  to do this. Once this has been achieved, the dissipative term in Equation (8) becomes significant and the energy decays.

Figure 5(a) examines the excitation of the first five Fourier modes in the plasma. Phase-mixing carries significant amounts of energy down to lower length-scales where the dissipative terms in Equation (8) can have a large effect, as expected from Equation (33). Figure 5(b) shows the excitation of increasing smaller Fourier modes with height  $z$ . As  $z$  increases, shorter length-scales are being created, as expected from Equation (3).

Note however, that the dissipative length-scale, represented in this particular example by Fourier mode  $m \sim 15$ , is not excited noticeably; most of the energy has dissipated away before a significant amount reaches it. Although only Fourier modes 1 to 20 are shown, the calculation was run using  $N \times N$  square matrices with  $N = 102$ , which more than adequately resolves the dissipative length-scale. The reason for this relatively poor penetration of energy down to finer length-scales can be seen if we consider the gradient of the Alfvén wavefront along the direction of the inhomogeneity. Taking  $\partial/\partial x$  of Equation (14) and comparing it to Equation (3), then

$$n \sim z, \quad (39)$$

i.e., length-scales appear linearly with height. Substituting this scaling into Equation (12) and asking for the value of  $n$  that causes the exponent to be of order unity, we obtain

$$n \sim R^{1/3}. \quad (40)$$

The smallest length-scale to be excited follows this approximate scaling with  $R$ . Hence we expect that Fourier modes higher than some particular limit are very highly damped and therefore cannot carry significant amounts of energy to yet shorter length-scales.

#### 4.2.2. *Strong Damping*

Here (Figure 4(d)), we calculate the energy evolution when  $R = 50$ . The energy decay (solid line) is faster than the Heyvaerts–Priest (dot-dot-dot-dashed line) or uniform decays (dot-dashed line). This is due to the appearance of smaller length-scales (Fourier modes  $m = 1, 2$  represented by the long and short-dashed lines, respectively) which dissipate faster. However, the relatively strong damping means that higher length-scales are damped very quickly and so higher length-scales are not greatly excited.

### 4.3. LENGTH-SCALE COUPLING

From the point of view of length-scale coupling, Alfvén wave evolution has so far only been considered for one case, namely nearest-neighbour length-scale coupling taking energy from the only initially excited Fourier mode, the fundamental.

Length-scales can be excited in a different manner by changing the inhomogeneity of the background Alfvén velocity. This alters the length-scale coupling in the phase mixing matrix  $\mathbf{P}$ . Changing the initial conditions will also change the length-scale excitation as this implies that energy is being introduced to the plasma at shorter length-scales. Coupling will still take place, but this time from modes having non-zero initial energy. The effect of varying these types of length-scale coupling is studied for conditions of strong phase-mixing and weak damping; i.e., we fix  $\delta = 0.5$  and  $R = 5000$  in Equation (34) and examine the wave evolution over the range  $0 \leq x \leq 1$ ,  $0 \leq k_0 z \leq 100$  and  $N = 102$ .

#### 4.3.1. Shorter Length-Scales Initially Excited

With initial condition  $u(x, 0) = \sin(5\pi x)$  and  $m = 1$  in Equation (34), energy is phase-mixed to both longer and shorter length-scales, as demonstrated in Figure 6(a). In Figure 6(b) the overall energy evolution (solid line), drops off initially following the purely dissipative behaviour (dot-dashed line). This gives the decay a head start on the Heyvaerts–Priest behaviour (dot-dot-dot-dashed line), which requires height to build up the shorter length-scales which are then dissipated. This analysis correctly takes account of the  $z = 0$  boundary condition. In the Heyvaerts–Priest analysis, the initial conditions are decoupled from the overall decay, i.e., all initial conditions evolve in the same way (Equation (12)), which the uniform case (Section 3.2) shows to be incorrect.

By putting in energy at shorter length-scales (compared to Sections 4.1 and 4.2), the plasma is excited at a length-scale which has a greater dissipative rate, according to Equation (33). Since energy is already appearing at short length-scales, phase-mixing is not required to carry energy down to those length-scales and so is not as important as in previous cases. Hence, the overall energy behaviour is dissipatively dominated for initial conditions carrying most of its energy at shorter length-scales.

#### 4.3.2. Phase-Mixing Matrix

The length-scale coupling inherent in the plasma can be manipulated using the background Alfvén velocity (34); for  $m = 5$ ,

$$v_A^2(x) = v_0^2 \left[ 1 + \delta \cos \left( \frac{5\pi x}{L} \right) \right], \quad (41)$$

which couples Fourier length-scales that differ in order by 5. This creates a phase-mixing matrix  $\mathbf{P}_*$ ,

$$[\mathbf{P}_*]_{mn} = \begin{cases} \delta & \text{if } m = n + 4 \text{ or } n = m + 4 \\ 0 & \text{otherwise,} \end{cases}$$

which is zero everywhere except on the fifth super- and sub-diagonals; elements in these positions are equal to  $\delta$ . The results of this coupling with initial condition  $u(x, 0) = \sin(\pi x)$  can be seen in Figures 6(c), 6(d), 7(a) and 8(a).

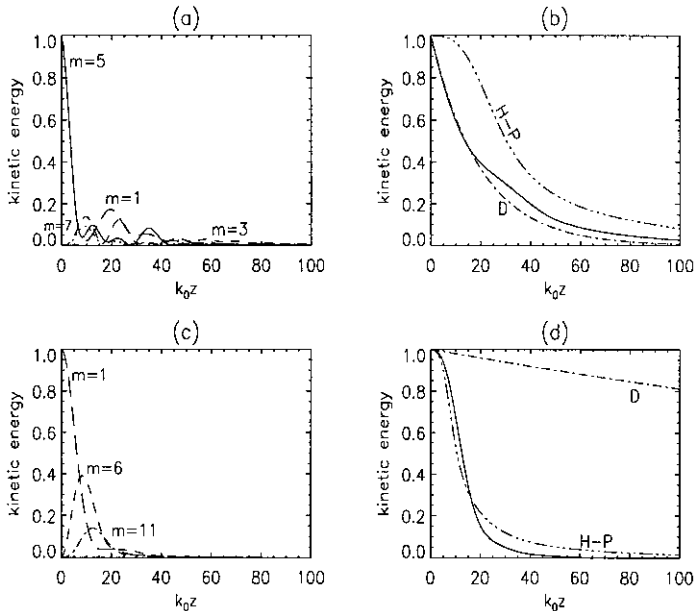


Figure 6. Effect of different length-scale coupling for strong phase-mixing and weak damping. (a) Length-scale excitation for  $u(x, 0) = \sin(5\pi x)$ , Fourier modes  $m = 1$  (long dashed line),  $m = 3$  (short dashed line),  $m = 5$  (solid line), and  $m = 7$  (dotted line). (b) Calculated energy evolution (solid line) compared to Heyvaerts–Priest (dot-dot-dot-dashed line) and uniform, dissipative (dot-dashed line) evolutions for  $u(x, 0) = \sin(5\pi x)$ . (c) Length-scale excitation for phase mixing matrix  $\mathbf{P}_*$ , Fourier modes  $m = 1$  (long dashed line),  $m = 6$  (short dashed line) and  $m = 11$  (dashed line). (d) Calculated energy evolution (solid line) compared to Heyvaerts–Priest (dot-dot-dot-dashed line) and uniform, dissipative (dot-dashed line) evolutions for phase-mixing matrix  $\mathbf{P}_*$ .

Figures 6(c) and 6(d) describe the energy evolution behaviour of the wave. Figure 6(d) compares the calculated energy decay to the Heyvaerts–Priest and purely dissipative decays. The Heyvaerts–Priest decay initially underestimates and then (at approximately  $k_0 z \sim 17$ ) overestimates the amount of energy present in the wave. Also, it is clear from Figure 8(a) that only four modes are significantly excited and that the calculation is well resolved.

Figure 7(a) demonstrates that the wave evolution is quite different from that expected by Heyvaerts and Priest (1983), shown in Figure 7(b). Sharp features are present at particular points in the wavefront due to the gradient in the background Alfvén velocity being zero at these points. This means that the strong phase-mixing condition Equation (11) is never satisfied, which implies that the Heyvaerts–Priest solution is not a good solution at these points, where the dissipative term should have a strong effect. We can therefore conclude that the Heyvaerts–Priest solution only partially includes the true effect of the  $\partial^2/\partial x^2$  term in Equation (8). Figure 7(a) correctly includes this term, which makes the wavefront much smoother in the direction of the inhomogeneity.

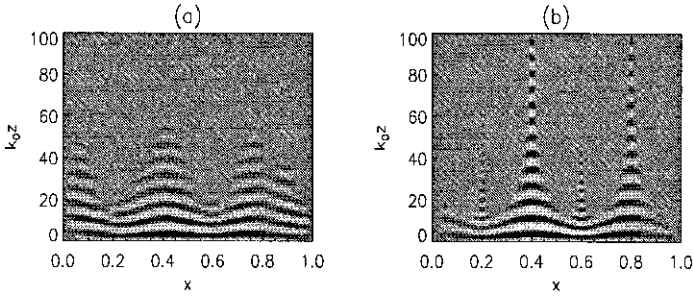


Figure 7. (a) Calculated wave evolution. (b) Heyvaerts–Priest wave evolution. Note the propagation of sharp features to large  $k_0 z$ .

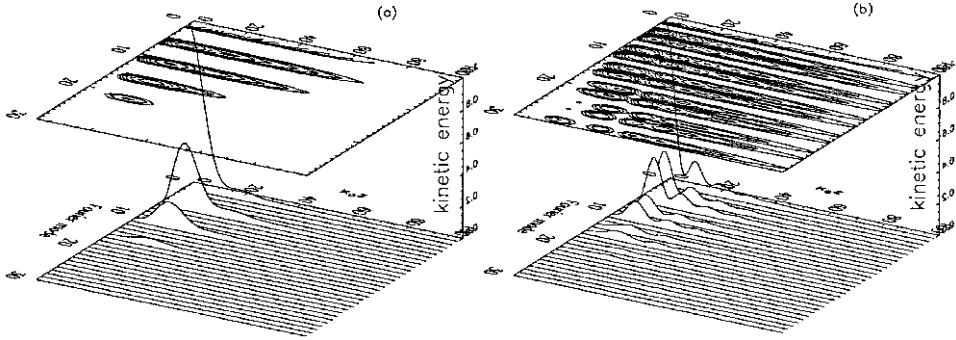


Figure 8. Length-scale excitation in (a) calculated wave evolution and (b) Heyvaerts–Priest solution.

A Fourier analysis of the Heyvaerts–Priest solution (Figure 8(b)) shows that many more length-scales are excited in their approximate solution than in the analysis presented here. In particular, energy is deposited at low heights into shorter length-scales, where it decays quickly, explaining the initial rapid decay of energy when compared to that caused by  $\mathbf{P}_*$  in this analysis. At larger  $z$ , Figure 8(b) shows that energy is significantly present at short length-scales, which causes the sharp features seen in Figure 7(b), where the Heyvaerts–Priest solution is not valid: short length-scales are being created but the subsequent damping is not correctly represented. However, the Heyvaerts–Priest solution does capture the important features of phase-mixing in a dissipative system: an initial build up of short length-scales due to phase-mixing leading to a rapid decay in wave amplitude and ending in a very gently decaying low amplitude tail.

#### 4.4. HIGHER VALUES OF $R$

As  $R$  increases towards coronal values, say  $R \geq 10^{10}$ , Equation (38) implies that the corresponding matrix must also increase in size as  $R^{1/2}$ : for example, to resolve the dissipative length-scale at say,  $R \sim 10^{10}$ , Equation (38) suggests that we have to have  $N \sim 10^5$ . This is because at higher  $R$  the effect of dissipation is weaker,

allowing significant amounts of energy to phase-mix to shorter length-scales. This means we must include more length-scales when solving the eigenproblem.

Consider the  $N \times N$  eigensystem  $\mathbf{M}_0$  (Equation (28)) for the ideal equation (1): this system describes nearest-neighbour length-scale coupling in a non-uniform, non-dissipative plasma. By Equation (39) this system is only valid up to a particular height. Consider now perturbing  $\mathbf{M}_0$  with the matrix

$$\mathbf{D} = \begin{bmatrix} r_1 & s_1 & 0 & 0 & \cdots & 0 & 0 \\ s_1 & r_2 & s_2 & 0 & \cdots & 0 & 0 \\ 0 & s_2 & r_3 & s_3 & \cdots & 0 & 0 \\ 0 & 0 & s_3 & r_4 & \cdots & 0 & 0 \\ \vdots & \vdots & \vdots & \vdots & \ddots & s_{N-2} & 0 \\ 0 & 0 & 0 & 0 & s_{N-2} & r_{N-1} & s_{N-1} \\ 0 & 0 & 0 & 0 & 0 & s_{N-1} & r_N \end{bmatrix}, \quad (42)$$

where  $r_n = -1 + 1/K_n^2$  and  $s_n = -1 + 1/K_n K_{n+1}$ . The system  $\mathbf{M}_0 + \mathbf{D}$  represents the first  $N$  length-scales in a dissipative phase-mixed Alfvén wave with nearest-neighbour length-scale coupling; its exact solution will give an exact answer for the Alfvén wave evolution up to a particular height. But that is not all. Equation (40) implies that there exists a value of  $N$  such that  $\mathbf{M}_0 + \mathbf{D}$  adequately resolves the Alfvén wave at all heights. This is because Fourier modes higher than  $N$  carry insufficient energy to affect the overall behaviour of the wave. However, for the large values of  $N$  implied by large  $R$ , standard solvers become unstable and therefore untrustworthy, and we are led to consider a perturbative approach.

Suppose we choose  $N$  such that  $\epsilon = \max[\mathbf{D}] = |r_N| \ll 1$ , and define  $\mathbf{C} = \mathbf{D}/r_N$ . Then for the  $n$ th eigenvector/eigenvalue we can write

$$[\mathbf{M}_0 + \epsilon \mathbf{C}] \mathbf{a}_n(\epsilon) = \lambda_n(\epsilon) \mathbf{a}_n(\epsilon). \quad (43)$$

For sufficiently small  $\epsilon$  we can write  $\lambda_n(\epsilon)$  and the corresponding eigenvector  $\mathbf{a}_n(\epsilon)$  as convergent power series, i.e.,

$$\lambda_n(\epsilon) = \xi_n + \sum_{k=1}^{\infty} \epsilon^k \zeta_{nk} \quad (44)$$

and

$$\mathbf{a}_n(\epsilon) = \mathbf{a}_n + \sum_{m=1}^{\infty} \sum_{k=1, k \neq n}^N \epsilon^m \eta_{mkm} \mathbf{a}_k, \quad (45)$$

respectively. The first-order in  $\epsilon$  corrections are

$$\zeta_{n1} = \frac{\mathbf{a}_n^T \mathbf{D} \mathbf{a}_n}{\mathbf{a}_n^T \mathbf{a}_n} \quad (46)$$

and for  $n \neq k$ ,

$$\eta_{nk1} = \frac{\mathbf{a}_n^T \mathbf{D} \mathbf{a}_k}{(\xi_n - \xi_k) \mathbf{a}_k^T \mathbf{a}_k} . \quad (47)$$

Note that we have had to fix  $N$  at such a value that  $\epsilon$  is small enough to allow this perturbation expansion to be valid. In practice, this value of  $N$  is found to be less than the value suggested by (40) due to perturbation expansion errors. Hence we are not adequately resolving the plasma at all heights. The effect of perturbation errors in the calculation is discussed below.

Initial conditions may also be recovered in a perturbation analysis. Let  $\mathbf{x}_0 = \mathbf{c} + \mathbf{d}$ , the initial conditions of Section 3.1. The eigenvector perturbation analysis above implies that the simultaneous equation problem is also perturbed. Define  $\mathbf{E}_m$  as

$$[\mathbf{E}_m]_{pn} = \sum_{k=1, k \neq n}^N \eta_{mkm} [\mathbf{a}_k]_p , \quad (48)$$

which is the  $m$ th-order perturbation matrix to the matrix of eigenvectors  $\mathbf{S}_0$ ;  $[\mathbf{E}_m]_{pn}$  is the  $m$ th order correction to the  $p$ th element of the  $n$ th eigenvector. The simultaneous equation problem becomes

$$\left[ \mathbf{S}_0 + \sum_{k=1}^{\infty} \epsilon^k \mathbf{E}_k \right] \left[ \mathbf{x}(0) + \sum_{k=1}^{\infty} \epsilon^k \mathbf{x}_k \right] = \mathbf{K} \mathbf{f}(0) = \mathbf{f}(0) + \sum_{k=1}^{\infty} \epsilon^k \mathbf{f}_k(0) . \quad (49)$$

This first-order correction to  $\mathbf{x}_0$  is

$$\mathbf{x}_1 = -\mathbf{S}_0 \mathbf{E}_1 \mathbf{x}_0 + \mathbf{S}_0 \mathbf{f}_1 , \quad (50)$$

since  $\mathbf{S}_0 = \mathbf{S}_0^{-1}$ .

To illustrate the results we can obtain using this method, we consider the profile of Equation (34) and calculate the evolution of such a wave in a plasma with  $R = 10^{10}$  on  $0 \leq k_0 z \leq 10000$  at two different values of  $N$ , namely  $N = 802$  and  $N = 1002$ . The calculated energy (Figure 9(a)) follows the Heyvaerts–Priest solution closely up until  $k_0 z \sim 3000$  and we conclude that this method gives good agreement with Heyvaerts and Priest (1983). The total energy at  $z = 0$  in Figure 9(a) is less than the true amount by about 1%, due to perturbation errors incorrectly recreating the initial conditions. After  $k_0 z \sim 3000$ , the two energy behaviours diverge. The reason for this may be seen in Figure 9(c). Energy propagates through down to shorter length-scales, taking energy out of the wave until the ‘energy front’ reaches the shortest available length-scale at  $N = 802$ . Since energy can no longer

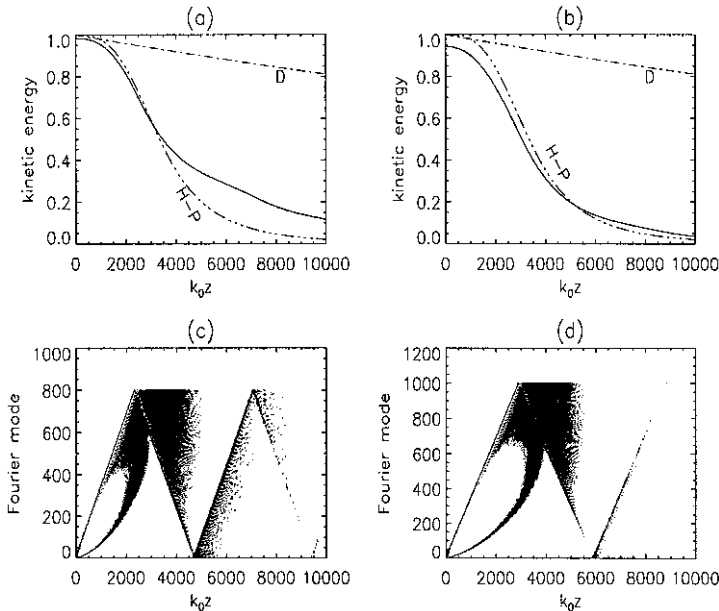


Figure 9. (a), (b) Calculated energy decay (solid line) for  $R = 10^{10}$  compared to Heyvaerts–Priest (dot-dot-dot-dashed line) and uniform, dissipative (dot-dashed line) cases for  $N = 802$  and  $N = 1002$ , respectively. (c) Contour plot of mode excitation versus height at kinetic energy  $= 1.0 \times 10^{-3}$  for  $R = 10^{10}$ ,  $N = 802$ . (d) Contour plot of mode excitation versus height at kinetic energy  $= 9.7 \times 10^{-3}$  for  $R = 10^{10}$ ,  $N = 1002$ .

propagate to shorter length-scales, it returns to longer length-scales. This type of energy return to longer length-scales is unphysical and it is this that causes the divergence of the calculated energy decay away from the Heyvaerts–Priest value.

Increasing  $N$  has two opposing effects in this treatment. In its favour, energy is allowed to propagate to shorter length-scales where it is more easily dissipated. This reduces the amount of energy available to ‘bounce-back’, and by Equation (39) it increases the height at which the wave may be resolved. However, increasing  $N$  also increases the value of  $\epsilon$  in the perturbation expansion. An important caveat in this treatment is that we may only use the above expansions for  $\epsilon$  sufficiently small (Wilkinson, 1965); what constitutes ‘small’ depends on the conditioning of the unperturbed problem. The calculation then begins to come up against the limits set by the perturbation expansion in both the eigenvector/eigenvalue and simultaneous linear equation problems (which may be tempered somewhat by including, say, second- and third-order terms in the calculation). This is demonstrated in the case  $N = 1002$  and shown in Figures 9(b) and 9(d). The total energy at  $k_0 z = 0$  in Figure 9(b) is about 6% less than the correct figure, again due to perturbation errors. However, the calculated energy decay clearly shows the Heyvaerts–Priest signature over a larger range of  $k_0 z$  than in the case  $N = 802$ . Figure 9(d) shows the unphysical energy ‘bounce-back’ encountered in Figure 9(c) occurring at a higher

value of  $k_0 z$ , as expected. Less energy is available to return to longer length-scales, improving the quality of the calculation at higher  $k_0 z$ .

In conclusion, there is a tradeoff between height and accuracy in this method. Small values of  $N$  will generate results that closely follow the Heyvaerts–Priest solution at low heights. Larger values of  $N$  allow the overall Heyvaerts–Priest decay to appear over a wider range of heights.

## 5. Conclusions

By applying a method first used by Cally (1991), we have been able to verify the Heyvaerts–Priest result for a phase-mixed Alfvén wave. Energy leaks out of the wave in this new analysis in approximately the same way as in an Heyvaerts–Priest wave. Combined with the results of Hood, Ireland and Priest (1997) this suggests that the  $\exp(-z^3)$  decay rate is a very robust result for this model. Hence this analysis in the strong phase-mixing, weak damping limit, agrees with the results of those papers, namely that Alfvén waves are indeed a viable mechanism for heating the solar corona.

However, there are some notable differences. This analysis properly takes account of the  $\partial^2/\partial x^2$  term in Equation (8), which is most striking in Section 4.3, where the length-scales directly excited have a profound effect on the wave evolution. When one considers Figures 7(a) and 7(b) (Section 4.3.2), it can be seen that the peaks in the Heyvaerts–Priest wave surface must be artifacts of the incomplete consideration of the diffusive derivative in the  $x$ -direction: it is precisely such sharp features that the phase-mixing of Alfvén waves in a diffusive plasma are meant to eliminate.

If smaller length-scales are present initially (Section 4.3.1), then these decay faster than the Heyvaerts–Priest rate, allowing a yet faster channel for the dissipation of Alfvén waves. From a coronal hole point of view, this channel is important to the heating only if the amount of energy available at scales smaller than the hole width is a significant proportion of the total energy available. This suggests that the presence of small, energetic structures at the base of coronal holes may be crucial in the overall Alfvénic heating of coronal holes. It should be noted that the observing programs BOUND (Insley, Moore, and Harrison, 1995) and BROAD (Harrison and Hassler, 1995) for the CDS (Coronal Diagnostic Spectrometer) instrument on board the SOHO (Solar and Heliospheric Observatory) platform are designed to look at small-scale structure and the presence of Alfvén waves in coronal holes. Such studies are vital in determining the likely contribution of phase-mixing to the coronal heating problem.

## References

- Browning, P. K. and Priest, E. R.: 1984, *Astron. Astrophys.* **131**, 283
- Cally, P. S.: 1991, *J. Plasma Phys.*, **45**, 453.
- Harrison, R. A. and Hassler, D.: 1995, in R. A. Harrison and A. Fludra (eds.), 'Enhanced Line Broadening with Altitude – [BROAD]', *The Coronal Diagnostic Spectrometer for the Solar and Heliospheric Observatory: Scientific Report*, August 1995.
- Heyvaerts, J. and Priest, E. R.: 1983, *Astron. Astrophys.* **117**, 220.
- Hood, A. W., Ireland, J., and Priest, E. R.: 1997, *Astron. Astrophys.*, in press.
- Insley, J., Moore, V., and Harrison, R. A.: 1995, in R. A. Harrison and A. Fludra (eds), 'Enhanced Line Broadening with Altitude – [BOUND]', *The Coronal Diagnostic Spectrometer for the Solar and Heliospheric Observatory: Scientific Report*, August 1995.
- Ionson, J. A.: 1978,, *Astrophys. J.* **226**, 650.
- Nocera, L., Leroy, B., and Priest, E. R.: 1984, *Astron. Astrophys.* **133**, 387.
- Wilkinson, J. H.: 1965, *The Algebraic Eigenvalue Problem*, Clarendon Press, Oxford, 1965.